Energy Materials

Article

Rotational angle detection with torsional quasi-zero stiffness design: precise mechanical sensing for energy harvesting

Xingjian Feng[#], Chongpu Zhai[#], Yifan Li, Yanyu Li, Haoyu Gu, Shaoqi Huang, Shuwen Zhang[*] [iD], Minglong Xu[*] [iD]

State Key Laboratory for Strength and Vibration of Mechanical Structures, School of Aerospace Engineering, Xi'an Jiaotong University, Xi'an 710049, Shaanxi, China.
[#]Authors contributed equally.

***Correspondence to:** Prof. Shuwen Zhang, State Key Laboratory for Strength and Vibration of Mechanical Structures, School of Aerospace Engineering, Xi'an Jiaotong University, No. 28, Xianning West Road, Xi'an 710049, Shaanxi, China. E-mail: shuwen@xjtu.edu.cn; Prof. Minglong Xu, State Key Laboratory for Strength and Vibration of Mechanical Structures, School of Aerospace Engineering, Xi'an Jiaotong University, No. 28, Xianning West Road, Xi'an 710049, Shaanxi, China. E-mail: mlxu@xjtu.edu.cn

Abstract

During mechanical energy harvesting, complicated mechanical loads are expected to be converted into electrical energy types, including compression, extension, torque, and the coupling of them. Mechanical energy harvesting evaluation is necessary, and it is normally applied by precise mechanical sensing, such as strain gauges and piezoelectric materials. The additional and changing equivalent stiffness of the sensing approach decreases the mechanical sensing precision, and then the energy harvesting evaluation is affected. This study introduces a method for torsional sensing with torsional quasi-zero stiffness (TQZS) structures by flexoelectricity. By designing the bending beam geometry, a structure with an extended TQZS range is developed, enabling enhanced mechanical and electrical performance. Within the TQZS loading range, the generated flexoelectric charges exhibit a robust linear relationship with structural deformation, providing precise monitoring capabilities for torsion-related mechanical quantities. By leveraging flexoelectric effect, the proposed structure also converts mechanical load into electrical signal, making it suitable for high-resolution sensing, helping energy harvesting applications.

Keywords: Torsional quasi-zero stiffness, flexoelectricity, energy harvesting, mechanical sensing

INTRODUCTION

Energy recycling and storage are paramount in contemporary society, with mechanical energy harvesting garnering significant interest due to its abundant availability, cost-effectiveness, ease of acquisition, and environmentally friendly nature. Mechanical energy sources such as sea waves, wind, vehicle brakes, and industrial device vibrations present immense potential for conversion into electrical energy. However, precise evaluation of mechanical-based deformation during energy harvesting remains crucial. During various mechanical engineering measurements, the demand for accuracy in mechanical Quantities measurement has been required, leading to a corresponding need for high-precision mechanical sensing with low equivalent stiffness[1-4]. To enhance mechanical sensing capabilities, various methods have been explored, including new material investigations[5], optimization of signal conversion efficiency[6], and nanomanufacturing techniques[7,8]. The increasing demand for monitoring periodic energy sources such as tidal and wind energy presents challenges for typical displacement sensors, as they are unable to avoid the impact on the measured system caused by additional stiffness[9,10].

To address the undesirable impact of additional stiffness on the measured system, quasi-zero stiffness (QZS) structures have been proposed and utilized[11-13]. These structures maintain QZS within its operating range and are applied in displacement measurements[14-16]. In the realm of mechanical quantities, the measurement of torsional angles is also crucial. Most current contact-based torsional angle sensors endure from the impact of additional torsional stiffness[17-19]. Eliminating additional torsional stiffness is very important. Directly applying the QZS structure to address the issue of additional torsional stiffness is not feasible, and hence torsional QZS (TQZS) structures are highly expected[20]. TQZS structure may be able to exhibit zero torsional stiffness. Within the TQZS working range, the structures typically undergo large deformations with significant strain gradients, which may generate flexoelectricity[21-23]. This electro-mechanical procedure converts mechanical deformations such as torsional angles into electrical signals from the TQZS structure, without introducing additional torsional stiffness[24].

Flexoelectric effect with typical TQZS structures enables detection and sensing of mechanical signals, particularly in scenarios involving non-uniform large deformations[25-27]. Flexoelectricity arises from strain gradients and is prevalent in all types of dielectric materials[28,29]. Flexoelectricity has the advantages of being non-limited by Curie temperature and size dependence, expecting the mechanical design and small dimensions[30,31]. It is able to be applied in force and displacement sensing operating under high-temperature ranges[32]. The combination of TQZS structures with the flexoelectric effect enables accurate sensing with no additional equivalent stiffness. Flexoelectricity is represented by

$$P = \mu_{ijkl} \frac{\partial \varepsilon_{ij}}{\partial x_k}, \tag{1}$$

where P is the flexoelectric polarization component, μ_{ijkl} is a fourth-order tensor representing the flexoelectric coefficient constant, ε_{ij} is the strain, and x_k is the position coordinate. The flexoelectric polarization induced by deformation of the equivalent charge center initially arises from non-uniform strain. For large deformation sensing, functional dielectric materials such as polymers and elastomers are expected with a large deformation range. Polymeric materials exhibit lower flexoelectric coefficients than ceramics, but the large strain and strain gradient responses make it suitable on sensing with flexoelectricity by designing large deformations. The flexoelectric electrical polarization can also be enlarged by the designed huge strain gradients[33].

This work proposes a mechanical torsion measurement method that combines the flexoelectric effect with TQZS structures and provides a mechanical sensing design, which is very important as it can improve the overall accuracy and reliability of the measurements.

DESIGN AND EXPERIMENTAL
Design of torque quasi-zero stiffness structure

This study adopts a structurally simplified bi-stable beam configuration. This configuration exploits intervals where the strain energy uniformly varies between the beam's two stable states. In an ideal TQZS structure, there is a plateau phase during the loading process where the torque remains constant despite an increase in the twist angle. Figure 1A illustrates the ideal TQZS loading curve, highlighting the TQZS plateau. The optimal operating range for the designed TQZS sensor corresponds to this TQZS plateau. A continuous bending beam structure is employed. Seamless transitions between bending beam segments ensure torque output continuity during deformation.

The axis of the continuous bending beam is shaped by four positioning points N_0, N_1, N_2, and N_3, along with the tangent control vectors at each positioning point, as shown in Figure 1B. The vector l_0 at point N_0 is radial to the circumference. The control vector at point N_1 forms an angle α_1 with the horizontal direction, with the magnitudes of the vectors being l_{1+} and l_{1-}. For simulation convenience to determine the optimal structure, these magnitudes are set equal to l_1. At N_2, curvature radius control is introduced, with a curvature radius of ρ. The vector angle at N_2 is α_2, and its vector magnitude is controlled by ρ and α_2, making it not an independent variable. The vector at N_3 forms an angle α_3 with the horizontal direction and has a magnitude of l_3.

As shown in Figure 1C, after determining the high-order spline curve that serves as the axis of the continuous bending beam, the beam is generated by assigning thickness and width. This design approach ensures the smoothness and continuity of the beam, effectively reducing stress concentration and maintaining the simplicity of the overall structure. To enhance the overall stability of the TQZS structure and balance the distribution of torque, a spoke-like structure is employed. Six symmetrically arranged bending beams are firmly attached between a central cylinder and a concentric hollow outer cylinder. The thickness t and the width S of the bending beams, the radius R_1 of the central cylinder, the outer radius R_2 of the hollow cylinder, and the thickness H_1 of the ring are provided in Table 1.

As shown in Figure 1A, the TQZS plateau is confined between points A and B. In accordance with the application conditions, the length of the TQZS plateau L_{TQZS}, the midpoint of the TQZS segment displacement θ_M, and the preload T_P are defined as follows:

$$\begin{cases} L_{TQZS} = \theta_B - \theta_A \\ \theta_M = \dfrac{1}{2}(\theta_A + \theta_B) \\ T_P = f(\theta_A) = f(\theta_M) = f(\theta_B) \end{cases}, \qquad (2)$$

In this design, θ_A, θ_B and θ_M denote the twist angles corresponding to points A, B, and their midpoint, respectively, while $F = f(x)$ represents the torque-angle function.

In experimental conditions, during the loading process of the TQZS structure, deformations such as cyclic torsion lead to the mutual cancellation of internal torque at energy inflection points within the structure. Consequently, the variation in external reactive torque is minimal, thus achieving the objective of QZS. In

Table 1. Geometries of the structure

Parameter	H_1	R_1	R_2	t	S
Value (mm)	2	15	77.5	1	15
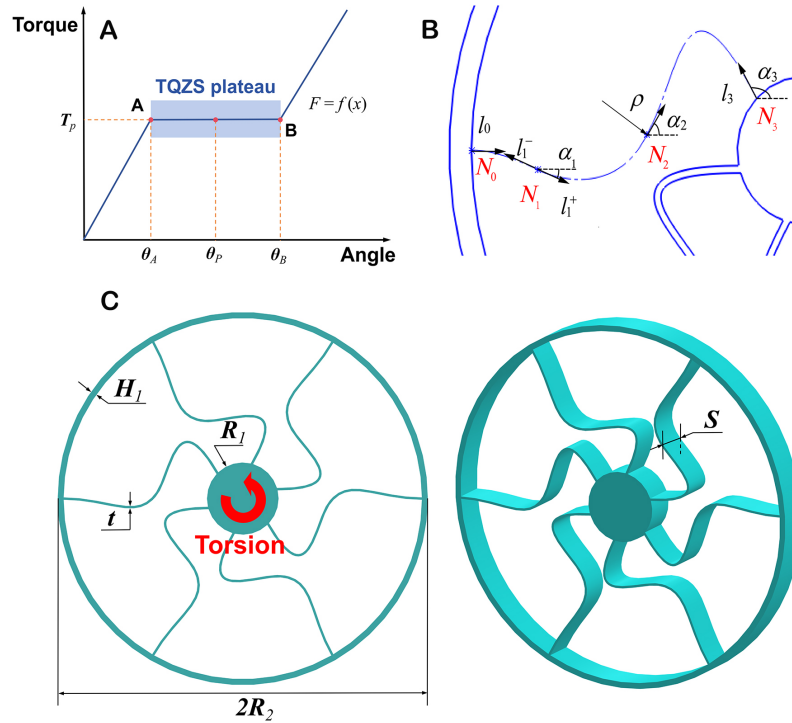
Figure 1. (A) Ideal torsional quasi-zero stiffness loading curve, (B) The proposed bending beam axis schematic, (C) The proposed TQZS structure schematic and the direction of applied torsion.

the torque-angle relation of the TQZS structure, we introduce a parameter ξ to quantify the flatness of the TQZS plateau, defined as:

$$\xi = \frac{T_{\min}}{T_{\max}},$$

(3)

where $T_{\min}$ and $T_{\max}$ represent the minimum and maximum torque values between the starting and ending points. Based on our previous work, to ensure that the designed TQZS structure has a relatively flat torque-twist angle plateau, we set ξ to be greater than or equal to 95% in subsequent simulations to determine the length of L_{TQZS}[34]. Meanwhile, T_{p} is redefined as the average of $T_{\min}$ and $T_{\max}$ for ease of comparison, defined as follows:

$$T_{\text{p}} = \frac{1}{2}\left(T_{\min} + T_{\max}\right),$$

(4)

The constructed model is analyzed using the Finite Element Method (FEM) with tetrahedral elements for meshing. To ensure the reliability of the results, an appropriate mesh size must be selected to guarantee convergence. We apply a load with an angle of 0.15 radians to the structure and use FEM to calculate the

average stiffness during the loading process. The results are shown in Figure 2. When the mesh size is less than or equal to 1.0 mm, the obtained results are all 101.281 mN·m/°, indicating that the results are convergent and reliable for mesh sizes less than or equal to 1.0 mm. Based on the results, The overall mesh size is set to 1 mm, while at the continuous bending beam, it is set to 0.2 m, which falls within the range, so we can consider the simulation results to be valid and reliable.

To ensure that the structure can withstand large deformations without yielding or fracturing, we selected high-strength nylon PA12 as the structural material. This material exhibits flexoelectric behavior similar to poly(vinylidene fluoride) (PVDF), which is widely utilized in research due to its high flexoelectric coefficient. The material properties of PA12, including density ρ_0, elastic modulus E, Poisson's ratio v, dielectric constant ε_r, and yield strength σ_y, are listed in Table 2. The external cylindrical surface is fixed, and a reference point is defined at the center of the upper surface of the small cylinder, coupled with the upper surface. The external torque will be applied to the reference point. Considering the range of beam deformation, geometric nonlinearity is activated during mechanical loading.

For each simulation, the torsional angle varies from 0° to 80° in 0.8° increments. To ignore the impacts from material viscosity and structural rotational acceleration, quasi-static simulation mode is applied for the analysis. Each simulation adjusts only one parameter while keeping others constant. TQZS plateau length L_{TQZS} and preload torque magnitude T_P are derived from the obtained torque-angle curves. After adjusting each parameter in the simulation, the normalized results for the TQZS plateau length L_{TQZS} and preload torque magnitude T_P are depicted in Figure 3 for intuitive representation.

From Figure 3A and B, it can be observed that the preload torque T_P decreases with the rise in the angle α_1 at control point N_1, while the plateau length L_{TQZS} initially increases and then decreases, reaching its maximum at 60°. As the vector magnitude l_1 grows, the preload torque T_P initially increases and then decreases, whereas the plateau length L_{TQZS} continuously decreases; however, the variations in both are relatively small.

From Figure 3C and D, it can be seen that the preload torque T_P shows a trend of decreasing first and then increasing with the increase in the angle α_2 at control point N_2, reaching its minimum at sixty degrees. The plateau length L_{TQZS} initially increases and then decreases, also reaching its minimum at 60°. As the curvature radius ρ at N_2 increases, the preload torque T_P slightly fluctuates, but the plateau length L_{TQZS} first rapidly increases and then sharply decreases, reaching its maximum at 75 mm.

Figure 3E and F shows that with the increase in the angle α_3 at control point N_3, the preload torque T_P first decreases rapidly and then more slowly, while the plateau length L_{TQZS} first increases and then decreases, reaching its maximum at 60°. With the increase in vector magnitude l_3, the preload torque T_P gradually decreases, and the plateau length L_{TQZS} first increases and then decreases, reaching its maximum at 45 mm; however, the variations in both are relatively small.

According to our previous work[34], the thickness t of the continuous bending beam mainly causes significant variations in preload torque T_P, which increases substantially with thickness, but does not significantly affect the length L_{TQZS} of the TQZS plateau[34]. To maximize the length of the TQZS plateau and rationalize the preload torque, parameters are selected based on the above simulation results as follows: beam thickness t = 1 mm, control vector angle α_1 = 45° and modulus l_1 = 5 mm at point N_1, control vector angle α_2 = 60° and curvature radius ρ = 75 mm at point N_2, and control vector angle α_3 = 60° and modulus l_3 = 45 mm at point N_3.

Table 2. The properties of PA12 nylon material

| Parameter	ρ_0	ν	E	ε_r	σ_y
Value (unit)	1.02 g/cm^3	0.4	1,420 MPa	3.1-5.0	60 MPa
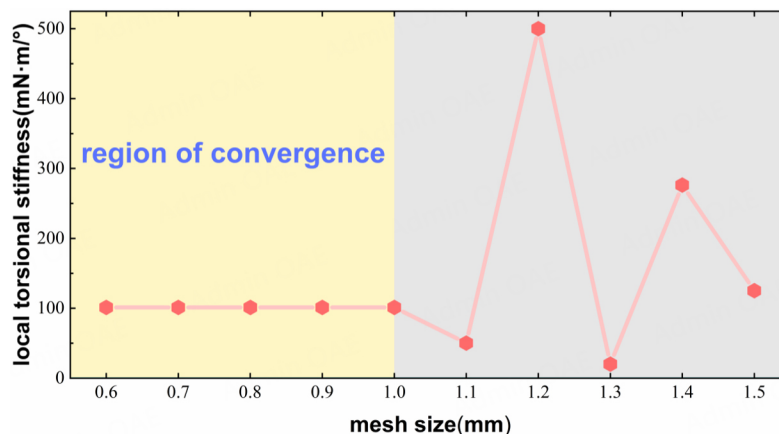
Figure 2. The relationship curve between mesh size and local torsional stiffness from FEM.

EXPERIMENTS

Based on the optimal TQZS structure obtained from the simulation, experiments are required to verify its feasibility and accuracy. Selective Laser Sintering (SLS) technology is employed to fabricate structures, achieving a precision of ±0.1 mm. To enlarge the flexoelectric charge output generated by the strain gradients across the entire structure, electrodes are applied over regions with concentrated strain gradients. Considering the significant impact of conventional patch electrodes on stiffness, a coating of conductive carbon paste is used as an alternative. This conductive carbon paste maintains flexibility and excellent conductivity, making it suitable for flexible electrodes. Comparative analysis demonstrates negligible differences in the mechanical response in torsional stiffness between coated and uncoated structures. The applications of low-amplitude vibrations and low-frequency oscillations are highly effective in capturing flexoelectric polarization charges while minimizing the strain hardening and viscous effects of the printing material. This approach ensures reliable measurement of flexoelectric polarization charges and enhances the overall performance of the printed structures.

At angular control mode, the loading system applies a torsional load followed by low-frequency oscillations, and records torque and angular displacement curves using built-in sensors. During oscillations, the total charge collected by the electrodes is amplified using a charge amplifier and recorded at a sampling rate of 520 Hz via an oscilloscope. At a controlled angular velocity of 1°/s, the stiffness curve of the tested structure is determined. The structure undergoes periodic reciprocating motion, starting from zero degrees and increasing the torsional amplitude in increments of 2.5° to measure the relationship between charge and torsional angle within the torsional bearing range.

To further investigate the relationship between deformation within the TQZS plateau and electrical signal output, the structure is compressed to the central angle θ_M and subjected to varying degrees of oscillations within the platform. During oscillations, the bending beam effectively undergoes cyclic bending, inducing cyclic flexoelectric polarization, and the corresponding polarization charge and mechanical signals are recorded. To enhance the signal-to-noise ratio, a low-pass filter with a cutoff frequency of 5 Hz is applied
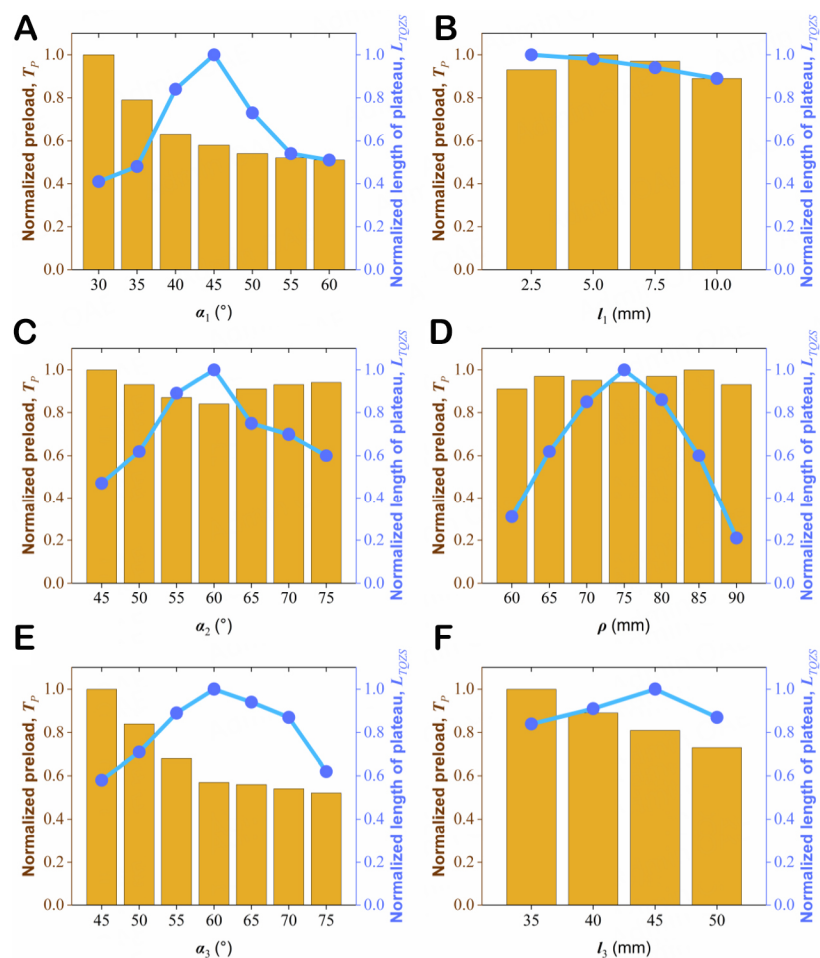
Figure 3. Factors affecting TQZS twist and pretension torque. (A) The angle between vectors at N_1, (B) The magnitude of the vector at N_1, (C) The angle between vectors at N_2, (D) The radius of curvature at N_2, (E) The angle between vectors at N_3, (F) The magnitude of the vector at N_3.

during data processing to remove noise. By identifying the peaks, troughs, frequencies, and other signal characteristics of charge, torque, and angular displacement, and correlating these signals with the electrical and mechanical responses of the TQZS structure, the output flexoelectric charges are separated. Given the negligible piezoelectric effect in nylon material, the influence of piezoelectricity is deemed insignificant.

More detailed experimental content can be found in Supplementary Table 1 and Supplementary Figure 1 of the Supplementary Materials.

RESULTS AND DISCUSSION

Figure 4 shows the initial state and strain contour plots under deformations from 10° to 80° from the FEM simulation results with the interval 10°, where the strain gradient directions are magnified. As illustrated in Figure 4, there are internal forces along the direction of the bending beam, inducing significant strain and strain gradients, which can generate considerable flexoelectric charges. The magnitude of these charges directly reflects the degree of structural deformation.
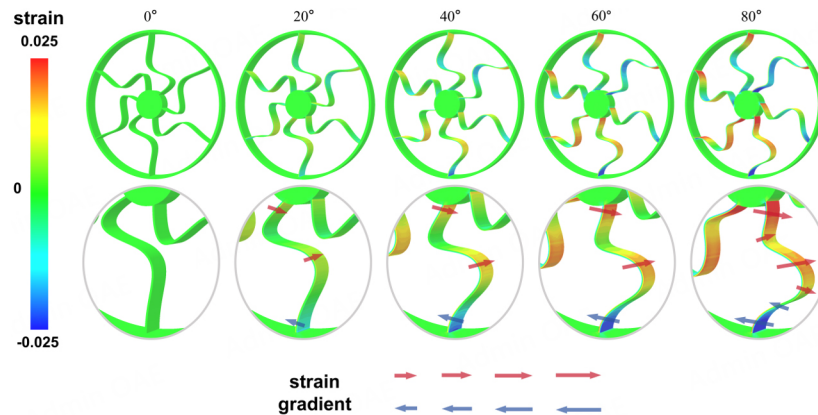
Figure 4. The initial state of the TQZS structure and the deformation shapes at certain angles during the deformation process, along with the corresponding local magnification of the beam deformation details, indicating the corresponding strain gradients.

The experimental results indicate that the TQZS platform L_{TQZS} = 20° and the TQZS central angle θ_M = 62.5°, as shown in Figure 5A. The finite element calculations are in good agreement with the experimental results. When the structure oscillates within the TQZS plateau range, the overall reactive torque variation is minimal, essentially maintaining quasi-zero torsional stiffness characteristics, as depicted in Figure 5B.

The charge measurement is divided into two parts. The first part explores the relationship between the charge and the torsional angle within the maximum torsional angle of the structure, with a linear fit shown in Figure 5C. The correlation coefficient exceeds 0.95, indicating a strong linear relationship between the charge output and the torsional angle. The second part examines the relationship between the charge and the torsional angle within the TQZS platform, as illustrated in Figure 5D. The correlation coefficient is also greater than 0.95, confirming a strong linear relationship between the charge and the torsional angle during the TQZS platform period. More detailed data can be found in Supplementary Figure 2 of the Supplementary Materials.

The observed high linearity and repeatability suggest that the proposed structure is promising for sensing torsional and other mechanical quantities. The proposed method measures the periodic oscillation of corresponding objects. Appropriately sized TQZS structures can be connected in series with the object. To ensure the structure remains in the TQZS state, pre-torsion is necessary. To achieve the maximum sensing range, it is recommended to twist the proposed structure to the center position of the TQZS platform period and use this position as the zero-point reference for torsional angle measurement, as shown in Figure 5D.

In this scenario, the sensing range is approximately half of the length of the TQZS platform. During the measurement process, the structure deforms with changes in the measured distance, generating flexoelectric polarization at the electrode positions, while the reactive torque remains essentially unchanged. In this work, the spoke-like structure effectively enhances structural stability and provides ample space for electrode coating, increasing polarization charge output and enhancing the robustness and sensitivity of the proposed structure. Importantly, the flexoelectric effect is not limited by the Curie temperature, allowing the proposed structure to function as a self-powering, absolute, and large-scale deformation sensing approach.

TQZS structures are realized by combining linear positive stiffness (> 0) elastic elements with nonlinear negative stiffness (< 0) elastic elements through specific mechanical and structural design. Negative stiffness
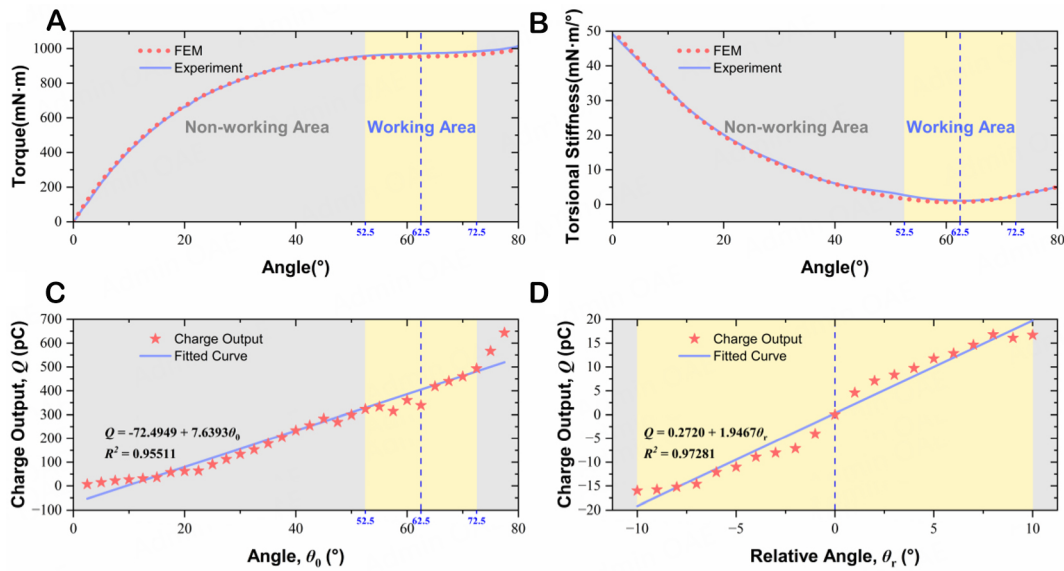
Figure 5. (A) Torque *vs.* torsional angle plot, (B) Torsional stiffness *vs.* torsional angle plot. (C) Output charge *vs.* the torsional angle. (D) Within the TQZS platform, with θ_M as the origin, the output charge *vs.* the relative torsional angle.

herein refers to a special mechanical property where the load varies inversely with deformations. Electromagnetic forces could be employed to achieve negative stiffness. Some design approaches for TQZS structures involves the TQZS plateau through nonlinear relationship between applied mechanical force and the induced deformation with specifically designed structures. This work utilizes the intermediate state of a bistable curved beam to achieve it and fine-tunes parameters to obtain an approximately optimal TQZS structure through its mechanical feedback.

Undoubtedly, material fatigue arising from multiple cyclic mechanical loading occurs during applications, especially onto those with strain gradients. These fatigue problems are mostly due to stress concentration and are closely related to materials and structures. To address this issue, materials with high fatigue strength are expected, and structural designs help alleviate stress concentration problems[35-38].

CONCLUSIONS

This work introduces a mechanical design method for rotational angle sensing utilizing a TQZS structure. By designing and optimizing the geometry of a bistable curved beam, a TQZS structure with a substantial range is achieved. The experimental results demonstrated a significant linear relationship between the generated flexoelectric charges and the structural deformation within the TQZS loading range, aligning well with finite element simulations. This study effectively combines quasi-zero torsional stiffness mechanical design with flexoelectric effect, enabling precise mechanical rotation sensing. This innovative approach allows for accurate detection of torsion-related mechanical quantities, showcasing its potential for energy harvesting applications, especially in capturing periodically varying energy sources. This work provides insight into high-resolution sensing, energy collection, and detection, underscoring the promising applications of TQZS structures in mechanical energy harvesting.

DECLARATIONS

have been crucial to the completion of this thesis. This work is supported by the National Natural Science Foundation of China (12002259).

Authors' contributions
Made substantial contributions to conception and design of the study and performed data analysis and interpretation: Feng, X.; Zhai, C.; Gu, H.; Zhang, S.
Performed data acquisition and provided administrative, technical, and material support: Feng, X.; Li, Y. (YiFan Li); Li, Y. (Yanyu Li); Huang, S.; Zhang, S.; Xu, M.

Availability of data and materials
The majority of the data supporting the findings of this study are included in the Supplementary Materials accompanying this article. The Supplementary Materials provides the necessary datasets and materials to validate most of the results presented in this study. For further inquiries, please contact the corresponding author.

Financial support and sponsorship
None.

Conflicts of interest
All authors declared that there are no conflicts of interest.

Ethical approval and consent to participate
Not applicable.

Consent for publication
Not applicable.

Copyright
© The Author(s) 2025.

REFERENCES

1. Wang, X.; Li, W.; Jin, L.; et al. High-precision micro-displacement sensor based on tunnel magneto-resistance effect. *Sci. Rep.* **2022**, *12*, 3021. DOI PubMed PMC
2. Babatain, W.; Bhattacharjee, S.; Hussain, A. M.; Hussain, M. M. Acceleration sensors: sensing mechanisms, emerging fabrication strategies, materials, and applications. *ACS. Appl. Electron. Mater.* **2021**, *3*, 504-31. DOI
3. Rodgers, M. M.; Pai, V. M.; Conroy, R. S. Recent advances in wearable sensors for health monitoring. *IEEE. Sensors. J.* **2015**, *15*, 3119-26. DOI
4. Wen, Q.; Li, P.; Zhang, Z.; Hu, H. Displacement measurement method based on double-arrowhead auxetic tubular structure. *Sensors* **2023**, *23*, 9544. DOI PubMed PMC
5. Brusa, E.; Carrera, A.; Delprete, C. A review of piezoelectric energy harvesting: materials, design, and readout circuits. *Actuators* **2023**, *12*, 457. DOI
6. Herrera-May, A. L.; Soler-Balcazar, J. C.; Vázquez-Leal, H.; Martínez-Castillo, J.; Vigueras-Zuñiga, M. O.; Aguilera-Cortés, L. A. Recent advances of MEMS resonators for lorentz force based magnetic field sensors: design, applications and challenges. *Sensors* **2016**, *16*, 1359. DOI PubMed PMC
7. Wei, L.; Kuai, X.; Bao, Y.; et al. The recent progress of MEMS/NEMS resonators. *Micromachines* **2021**, *12*, 724. DOI PubMed PMC
8. Liu, H.; Zhong, J.; Lee, C.; Lee, S. W.; Lin, L. A comprehensive review on piezoelectric energy harvesting technology: materials, mechanisms, and applications. *Appl. Phys. Rev.* **2018**, *5*, 041306. DOI
9. Shaw, A. D.; Gatti, G.; Gonçalves, P. J. P.; Tang, B.; Brennan, M. J. Design and test of an adjustable quasi-zero stiffness device and its use to suspend masses on a multi-modal structure. *Mech. Syst. Signal. Proc.* **2021**, *152*, 107354. DOI
10. Zhao, T.; Xu, M.; Xiao, X.; Ma, Y.; Li, Z.; Wang, Z. L. Recent progress in blue energy harvesting for powering distributed sensors in ocean. *Nano. Energy.* **2021**, *88*, 106199. DOI

11.   Cheng, C.; Li, S.; Wang, Y.; Jiang, X. Force and displacement transmissibility of a quasi-zero stiffness vibration isolator with geometric nonlinear damping. *Nonlinear. Dyn.* **2017**, *87*, 2267-79. DOI

12.   Sun, X.; Jing, X.; Cheng, L.; Xu, J. A 3-D quasi-zero-stiffness-based sensor system for absolute motion measurement and application in active vibration control. *IEEE/ASME. Trans. Mechatron.* **2015**, *20*, 254-62. DOI

13.   Ma, Z.; Zhou, R.; Yang, Q. Recent advances in quasi-zero stiffness vibration isolation systems: an overview and future possibilities. *Machines* **2022**, *10*, 813. DOI

14.   Zhang, C.; He, J.; Zhou, G.; Wang, K.; Xu, D.; Zhou, J. Compliant quasi-zero-stiffness isolator for low-frequency torsional vibration isolation. *Mech. Mach. Theory.* **2023**, *181*, 105213. DOI

15.   Huang, X.; Liu, X.; Sun, J.; Zhang, Z.; Hua, H. Effect of the system imperfections on the dynamic response of a high-static-low-dynamic stiffness vibration isolator. *Nonlinear. Dyn.* **2014**, *76*, 1157-67. DOI

16.   Zhou, J.; Xu, D.; Bishop, S. A torsion quasi-zero stiffness vibration isolator. *J. Sound. Vib.* **2015**, *338*, 121-33. DOI

17.   Schüthe, T.; Riemschneider, K. R.; Meyer-Eschenbach, A. Signal processing using a circular sensor array to measure the torsional angle of a bolted joint. *Sensors* **2024**, *24*, 2719. DOI PubMed PMC

18.   Homišin, J.; Kaššay, P.; Urbanský, M.; Puškár, M.; Grega, R.; Krajňák, J. Electronic constant twist angle control system suitable for torsional vibration tuning of propulsion systems. *J. Mar. Sci. Eng.* **2020**, *8*, 721. DOI

19.   Park, Y. H.; Lee, H. B.; Kim, G. W. Crack monitoring in rotating shaft using rotational speed sensor-based torsional stiffness estimation with adaptive extended kalman filters. *Sensors* **2023**, *23*, 2437. DOI PubMed PMC

20.   Zheng, Y.; Zhang, X.; Luo, Y.; Zhang, Y.; Xie, S. Analytical study of a quasi-zero stiffness coupling using a torsion magnetic spring with negative stiffness. *Mech. Syst. Signal. Proc.* **2018**, *100*, 135-51. DOI

21.   Abdollahi, A.; Peco, C.; Millán, D.; Arroyo, M.; Arias, I. Computational evaluation of the flexoelectric effect in dielectric solids. *J. Appl. Phys.* **2014**, *116*, 093502. DOI

22.   Abdollahi, A.; Arias, I. Constructive and destructive interplay between piezoelectricity and flexoelectricity in flexural sensors and actuators. *J. Appl. Mech.* **2015**, *82*, 121003. DOI

23.   Shen, S.; Hu, S. A theory of flexoelectricity with surface effect for elastic dielectrics. *J. Mech. Phys. Solids.* **2010**, *58*, 665-77. DOI

24.   Zhou, J.; Wang, X.; Xu, D.; Bishop, S. Nonlinear dynamic characteristics of a quasi-zero stiffness vibration isolator with cam-roller-spring mechanisms. *J. Sound. Vib.* **2015**, *346*, 53-69. DOI

25.   Wang, B.; Gu, Y.; Zhang, S.; Chen, L. Q. Flexoelectricity in solids: progress, challenges, and perspectives. *Prog. Mater. Sci.* **2019**, *106*, 100570. DOI

26.   Huang, W.; Yan, X.; Kwon, S. R.; Zhang, S.; Yuan, F. G.; Jiang, X. Flexoelectric strain gradient detection using $Ba_{0.64}Sr_{0.36}TiO_3$ for sensing. *Appl. Phys. Lett.* **2012**, *101*, 252903. DOI

27.   Ma, W.; Cross, L. E. Flexoelectric polarization of barium strontium titanate in the paraelectric state. *Appl. Phys. Lett.* **2002**, *81*, 3440-2. DOI

28.   Huang, S.; Qi, L.; Huang, W.; Shu, L.; Zhou, S.; Jiang, X. Flexoelectricity in dielectrics: materials, structures and characterizations. *J. Adv. Dielect.* **2018**, *8*, 1830002. DOI

29.   Meng, Y.; Chen, G.; Huang, M. Piezoelectric materials: properties, advancements, and design strategies for high-temperature applications. *Nanomaterials* **2022**, *12*, 1171. DOI PubMed PMC

30.   Kwon, S. R.; Huang, W. B.; Zhang, S. J.; Yuan, F. G.; Jiang, X. N. Flexoelectric sensing using a multilayered barium strontium titanate structure. *Smart. Mater. Struct.* **2013**, *22*, 115017. DOI

31.   Ma, W.; Cross, L. E. Large flexoelectric polarization in ceramic lead magnesium niobate. *Appl. Phys. Lett.* **2001**, *79*, 4420-2. DOI

32.   Ji, H.; Zhang, S.; Liu, K.; et al. Flexoelectric enhanced film for an ultrahigh tunable piezoelectric-like effect. *Mater. Horiz.* **2022**, *9*, 2976-83. DOI

33.   Zhou, Y.; Liu, J.; Hu, X.; Chu, B.; Chen, S.; Salem, D. Flexoelectric effect in PVDF-based polymers. *IEEE. Trans. Dielect. Electr. Insul.* **2017**, *24*, 727-31. DOI

34.   Gu, H.; Ji, H.; Zhang, S.; Zhai, C.; Xu, M. Displacement sensing with quasi-zero stiffness structure and flexoelectricity. *Smart. Mater. Struct.* **2023**, *32*, 035024. DOI

35.   Suresh, S.; Ritchie, R. O. Propagation of short fatigue cracks. *Int. Metals. Rev.* **1984**, *29*, 445-75. DOI

36.   Zheng, D.; Rosenberger, A.; Ghonem, H. Influence of prestraining on high temperature, low frequency fatigue crack growth in superalloys. *Mater. Sci. Eng. A.* **1993**, *161*, 13-21. DOI

37.   Chen, Y.; Monteiro, E.; Koutiri, I.; Favier, V. Fatigue-constrained topology optimization using the constrained natural element method. *Comput. Methods. Appl. Mech. Eng.* **2024**, *422*, 116821. DOI

38.   Slebioda, M.; Giele, R.; Langelaar, M. Topology optimization for infinite fatigue life of cyclic symmetric structures subjected to non-proportional loading. *Comput. Struct.* **2023**, *286*, 107113. DOI